Available online at www.sciencedirect.com
SCIENCE DIRECT®
Acta Materialia 53 (2005) 173–183
Acta MATERIALIA
www.actamat-journals.com

Thermodynamic description and unidirectional solidification of eutectic organic alloys: IV. Binary systems neopentylglycol–succinonitrile and amino-methyl-propanediol–succinonitrile

V.T. Witusiewicz *, L. Sturz, U. Hecht, S. Rex

Department of Materials and Processes, ACCESS e. V., Intzestrasse 5, D-52072 Aachen, Germany

Received 14 July 2004; received in revised form 31 August 2004; accepted 4 September 2004
Available online 26 October 2004

Abstract

The temperature and enthalpy of transformations of organic alloys from the binary systems neopentylglycol–succinonitrile (NPG–SCN) and 2-amino-2-methyl-1,3-propanediol–succinonitrile (AMPD–SCN) were measured by means of differential scanning calorimetry (DSC). The phase diagrams of these binary systems were assessed via the CALPHAD approach using Thermo-Calc by simultaneously optimizing the thermodynamic and phase equilibrium data measured in the present work. Proper agreements between the experimental and calculated data for the phase diagrams as well as for the thermochemical properties were achieved. Experiments and calculations show that both the NPG–SCN and the AMPD–SCN systems exhibit a non-variant eutectic reaction with the eutectic point at 90.45 mol% SCN (318.0 K) and at 97.39 mol% SCN (325.7 K), respectively. In the NPG–SCN system the temperature of the eutectic reaction is about 3 K higher than the temperature of the transformation from the ordered crystals (OCs) to the orientationally disordered crystals (ODICs), whereas the eutectic reaction in the AMPD–SCN involves the OCs of AMPD and the ODICs of SCN.

Unidirectional solidification experiments were performed with selected NPG–SCN and AMPD–SCN alloys in order to verify phases involved in solid–liquid equilibria and the nature of eutectic growth in these systems. We find that eutectic growth in NPG–SCN eutectic alloy occurs with both solid phases being non-facetted and with a rod-like eutectic structure. The eutectic as well as some hypo-eutectic alloys from the AMPD–SCN system show irregular eutectic growth with a non-facetted BCC_A2 phase of SCN and a facetted monoclinic phase of AMPD.

Keywords: Neopentylglycol–succinonitrile; Amino-methyl-propanediol–succinonitrile; Binary system; Thermodynamic description; Bridgman solidification; Eutectic growth

1. Introduction

In the previous parts of our work addressing the thermodynamic description of binary organic alloy systems we published experimental measurements, the CALPHAD description of the phase equilibria and unidirectional solidification experiments of the eutectic alloys in the binary systems succinonitrile (SCN) [1]–(D)camphor (DC) [2] [1], neopentylglycol (NPG) [3]–amino-methyl-propanediol (AMPD) [4] [2], NPG–DC [3] and

* Corresponding author. Tel.: +49 241 8098007; fax: +49 241 38578.
E-mail address: victor@access.rwth-aachen.de (V.T. Witusiewicz).

[1] Butanedinitrile, CAS No. [110-61-2].
[2] (1*R*)-1,7,7-Trimethylbicyclo[2,2,1]heptan-2-one, CAS No. [464-49-3].
[3] 2,2-Dimethyl-1,3-propanediol, CAS No. [126-30-7].
[4] 2-Amino-2-methyl-1,3-propanediol, CAS No. [115-69-5].

1359-6454/$30.00
doi:10.1016/j.actamat.2004.09.014

Table 1
DSC data on temperature and enthalpy of transformations of NPG–SCN alloys

SCN (mole fraction)	Transformation temperatures (K)			Enthalpy of transformation (J mol^{-1})			
	OCs/ODICs	Solidus	Liquidus	OCs/ODICs	Melting	Eutectic	Primary phase
0.000	314.5 [8]	–	403.3 [7]	12,520 [7]	4440 [7]	–	4440 [7]
0.000	315.0 [2]	–	403.2 [2]	12,061 [2]	4431 [2]	–	4431 [2]
0.039	315.9	317.3	399.8	12,106	4287	136	4151
0.146	316.1	320.3	381.5	10,811	4613	801	3811
0.254	315.8	317.9	368.8	9559	4829	1397	3432
0.294	314.1	316.6	364.9	8832	4696	1099	3597
0.313	314.2	319.0	366.1	8961	4448	1470	2978
0.418	313.5	318.0	361.3	7182	4667	1773	2894
0.418	313.5	318.2	361.3	7380	4755	1817	2938
0.499	313.4	318.8	359.7	6661	4964	2334	2630
0.503	314.3	316.9	356.0	5789	4819	2443	2376
0.560	313.9	317.3	353.3	5250	4688	2629	2058
0.607	314.4	318.5	353.7	4596	4810	2938	1872
0.665	315.9	318.4	352.6	3844	4725	3064	1661
0.699	314.3	317.2	347.9	3947	4766	3466	1301
0.713	315.6	317.8	347.0	3623	4531	3395	1136
0.754	314.1	316.9	340.9	3260	4888	3598	1290
0.817	314.1	317.7	338.5	2171	4666	3993	673
0.857	315.0	317.9	332.6	1870	4660	4133	527
0.898	314.6	318.5	321.0	1287	4611	4207	405
0.898	314.4	318.3	319.9	1077	4576	4282	294
0.899	313.9	317.3	320.4	1210	4270	4270	0
0.900	315.9	318.1	321.8	1207	4279	4265	14
0.905	312.7	317.1	317.1	1008	4658	4658	0
0.906	315.1	317.6	317.6	998	4515	4308	0
0.913	312.9	317.3	320.7	778	4230	4045	186
0.946	314.7	318.2	324.2	668	4302	3013	1289
0.949	314.0	317.4	325.4	303	3903	2536	1366
0.963	313.3	316.7	326.4	244	3937	1484	2454
0.974	314.0	318.3	329.4	296	4396	1086	3013
1.000	–	–	331.7	–	3693	–	3693
1.000	–	–	331.3 [1]	–	3610 [1]	–	3610 [1]
1.000	233.1 [5]	–	331.23 [6]	–	3703 [5]	–	3703 [5]

AMPD–DC [3]. All these investigations aimed to achieve a thermodynamic description of the quaternary organic alloy system AMPD–NPG–DC–SCN [4] intended to be used for in situ observation and numerical modelling of multicomponent eutectic growth in univariant and non-variant reactions.

The present work addresses investigations by means of experiments and computational thermodynamics with the last two constituent binary systems of the above named quaternary system, namely NPG–SCN and AMPD–SCN. To our best knowledge, for both systems no phase diagram and thermochemical data have been reported in literature.

In the present paper the NPG–SCN and AMPD–SCN phase diagrams, the enthalpy of transformation from the ordered crystals (OCs) to the orientationally disordered crystals (ODICs) and the enthalpy of fusion of different alloys were determined by differential scanning calorimetry (DSC). The obtained thermodynamic and phase equilibria data for both systems were consistently described via the CALPHAD approach. The model parameters have been evaluated using a computer optimisation technique based on the descriptions of the Gibbs energy of all individual phases of the pure AMPD, NPG and SCN substances proposed in the previous parts of the work [1,2]. Moreover, selected alloys of the NPG–SCN and AMPD–SCN systems were investigated by unidirectional solidification using the Bridgman technique in order to verify phases involved in solid–liquid equilibria and the nature of eutectic growth in these systems.

The purification and characterisation of pure substances, the procedures for preparation and alloying of the samples, the DSC and unidirectional solidification techniques and measuring procedures were the same as previously described in [1,4].

2. Results

2.1. DSC-measurements

Tables 1 and 2 summarise the results of the DSC measurements for different alloys of the NPG–SCN and the AMPD–SCN systems, respectively. The tables

Table 2
DSC data on temperature and enthalpy of transformations of AMPD–SCN alloys

SCN (mole fraction)	Transformation temperatures (K)			Enthalpy of transformation (J mol^{-1})		
	Solidus	OCs/ODICs	Liquidus	Melting + OCs/ODICs	Eutectic	Primary phase
0.000	–	352.89 [9]	384.1 [9]	26,280 [9]	–	2780 [9]
0.000	–	352.9 [2]	383.5 [2]	26,525 [2]	–	2745 [2]
0.036	334.0	352.9	372.5	23,071	0	23,071
0.043	332.1	355.1	372.7	23,314	0	23,314
0.083	325.7	357.7	362.5	21,527	417	21,110
0.088	323.7	–	368.3	21,742	239	21,503
0.126	322.4	351.9	357.0	21,377	443	20,934
0.166	323.3	–	355.4	19,758	517	19,241
0.181	321.3	353.3	357.0	19,680	341	19,339
0.224	324.5	–	355.2	20,119	998	19,121
0.242	325.6	–	354.1	19,410	–	–
0.256	327.9	–	353.3	18,949	693	18,256
0.265	325.0	–	353.4	19,003	881	18,122
0.304	327.3	–	352.8	17,226	1040	16,186
0.337	324.0	–	353.7	17,992	1026	16,966
0.397	325.1	–	352.0	15,686	1113	14,573
0.414	324.8	–	354.7	16,671	1545	15,126
0.449	323.8	–	351.5	16,008	1895	14,113
0.460	324.6	–	352.1	14,896	2075	12,821
0.503	324.5	–	352.0	13,978	1801	12,177
0.515	326.7	–	352.4	13,528	2051	11,477
0.569	324.6	–	351.4	12,237	2226	10,011
0.570	326.1	–	350.9	13,039.	2030	11,009
0.593	326.9	–	351.5	13,534	2430	11,104
0.597	324.8	–	352.7	12,514	2966	9548
0.607	323.9	–	352.0	11,894	2743	9151
0.664	325.6	–	351.4	10,764	2806	7958
0.693	321.7	–	350.3	11,003	3046	7957
0.698	326.0	–	350.6	11,884	3812	8072
0.731	325.4	–	350.8	9847	2894	6953
0.753	325.6	–	349.9	9722	3494	6228
0.754	325.2	–	350.9	9652	2881	6771
0.797	325.7	–	350.6	8800	3652	5148
0.832	326.5	–	347.9	7563	3554	4009
0.840	324.4	–	349.6	6999	3532	3467
0.852	323.3	–	347.9	7994	3622	4372
0.896	326.2	–	347.5	6483	3912	2571
0.920	325.8	–	347.5	6037	3768	2269
0.922	326.3	–	345.5	5419	4294	1125
0.938	326.3	–	342.2	5136	3961	1175
0.961	324.8	–	336.2	5666	4502	1164
0.961	325.2	–	336.8	4361	3956	405
0.967	326.3	–	333.0	4072	3820	252
0.985	325.0	–	327.3	3799	2986	813
0.989	324.0	–	326.0	3618	307	3311
1.000	–	–	331.7	3693	–	3693
1.000	–	–	331.3 [1]	3610 [1]	–	3610 [1]
1.000	–	233.15 [5]	331.23 [6]	3703 [5]	–	3703 [5]

give the temperatures of the OCs/ODICs phase transitions, the solidus and liquidus temperatures and the values of the enthalpy of phase transitions. The values for pure substances available in literature [1,2,5–9] are given as well for comparison with the data obtained in the present work. To better separate the contributions of the OCs/ODICs phase transformation, the eutectic reaction and the melting/solidification of the primary phase to the enthalpy of transformation in NPG–SCN alloys, the DSC cooling curves with a scanning rate of 3 K min^{-1} were used in addition to the DSC heating curves. Peaks on the cooling curve relating to these transitions in NPG–SCN alloys separate well due to deep undercooling of the eutectic and the kinetic suppression of the OCs/ODICs transformation. For the case of AMPD–SCN alloys it was impossible to correctly separate the enthalpy of transformation related to the monoclinic/BCC_A2 transformation from the enthalpy

of melting, because the peaks related to these transitions strongly overlap.

2.2. Thermodynamic modelling

2.2.1. Pure substances

The descriptions of the Gibbs energy of the pure substances AMPD, NPG and SCN in the form GH^{SER} [10] were published in our previous work [1,2].

2.2.2. Solution phases

All phases of the binary NPG–SCN and AMPD–SCN alloy systems are modelled as substitutional solutions. No new phases, other than those pertaining to the pure substances were found in these binary systems.

The lattice stability and the thermodynamic parameters for all individual phases were found by means of thermodynamic optimisation utilizing all data regarding phase equilibria and thermochemical properties measured by DSC. Note, that the monoclinic phase which is present in each pure substance was modelled by one set of parameters creating appropriate composition sets. The optimisation was carried out using the *PARROT* module of the Thermo-Calc software [11].

2.2.3. Optimisation results and discussion

The evaluated thermodynamic parameters for the NPG–SCN and AMPD–SCN systems are listed in Table 3 and all nonvariant reactions found are summarised in Table 4. The calculated phase diagrams for the NPG–SCN and the AMPD–SCN systems according to

Table 3
Summary of the thermodynamic parameters of the solution phases of the NPG–SCN and AMPD–SCN systems (in J mol^{-1})

Phase	Parameter
NPG–SCN system	
Liquid	${}^0L^{\mathrm{LIQ.}}_{\mathrm{NPG,SCN}} = 4735 + 3.787\ T$
	${}^1L^{\mathrm{LIQ.}}_{\mathrm{NPG,SCN}} = -3499 + 9.915\ T$
	${}^2L^{\mathrm{LIQ.}}_{\mathrm{NPG,SCN}} = 4976 - 12.273\ T$
FCC_A1	${}^0G^{\mathrm{FCC\_A1}}_{\mathrm{SCN}} - H^{\mathrm{SER}}_{\mathrm{SCN}} = 1720 + \mathrm{GH}^{\mathrm{SER}}_{\mathrm{SCN}}$
	${}^0L^{\mathrm{FCC\_A1}}_{\mathrm{NPG,SCN}} = 9030$
BCC_A2	${}^0G^{\mathrm{BCC\_A2}}_{\mathrm{NPG}} = 550 + {}^0G^{\mathrm{FCC\_A1}}_{\mathrm{NPG}}$ [2]
	${}^0L^{\mathrm{BCC\_A2}}_{\mathrm{NPG,SCN}} = 12,241$
Monoclinic	${}^0L^{\mathrm{MONOCL.}}_{\mathrm{NPG,SCN}} = 7900$
NPG-III	${}^0G^{\mathrm{NPG\text{-}III}}_{\mathrm{SCN}} - H^{\mathrm{SER}}_{\mathrm{SCN}} = 3300 + \mathrm{GH}^{\mathrm{SER}}_{\mathrm{SCN}}$
	${}^0L^{\mathrm{NPG\text{-}III}}_{\mathrm{NPG,SCN}} = 7700$
AMPD–SCN system	
Liquid	${}^0L^{\mathrm{LIQ.}}_{\mathrm{AMPD,SCN}} = 3111 + 9.807\ T$
	${}^1L^{\mathrm{LIQ.}}_{\mathrm{AMPD,SCN}} = -1530 + 3.945\ T$
	${}^2L^{\mathrm{LIQ.}}_{\mathrm{AMPD,SCN}} = 5497 - 11.114\ T$
BCC_A2	${}^0L^{\mathrm{BCC\_A2}}_{\mathrm{AMPD,SCN}} = 7545 + 23.656\ T$
	${}^1L^{\mathrm{BCC\_A2}}_{\mathrm{AMPD,SCN}} = -4939$
Monoclinic	${}^0L^{\mathrm{MONOCL.}}_{\mathrm{AMPD,SCN}} = 19,508 - 38.461\ T$
AMPD-II	${}^0G^{\mathrm{AMPD-II}}_{\mathrm{SCN}} - H^{\mathrm{SER}}_{\mathrm{SCN}} = 1500 + \mathrm{GH}^{\mathrm{SER}}_{\mathrm{SCN}}$
	${}^0L^{\mathrm{AMPD-II}}_{\mathrm{AMPD,SCN}} = 15,800$

Table 4
Nonvariant reactions in NPG–SCN and AMPD–SCN systems

Reaction between phases	Type	T (K)	Phase composition, x_{SCN}			Rem.
$\phi_1/\phi_2/\phi_3$			ϕ_1	ϕ_2	ϕ_3	
NPG–SCN system						
Liquid ↔ FCC_A1 + BCC_A2	Eutectic	317.8 ± 0.8	0.90 ± 0.01	0.01 ± 0.01	0.99 ± 0.01	Exp.
		318.0	0.905	0.019	0.992	Calc.
FCC_A1 ↔ Monocl.#1 + BCC_A2	Eutectoid	314.4 ± 0.9	0.02 ± 0.01	0.02 ± 0.01	0.99 ± 0.01	Exp.
		314.8	0.019	0.025	0.992	Calc.
BCC_A2 + Monocl.#1 ↔ Monocl.#2	Peritectoid	234.6	1.000	0.020	0.980	Calc.
Monocl.#1 ↔ NPG-III	Allotropic	60.4	0.000	0.000	–	Calc.
AMPD–SCN system						
Liquid + BCC_A2 ↔ Monocl.#1	Peritectic	354.2 ± 2.3	0.20 ± 0.03	–	0.04 ± 0.01	Exp.
		354.4	0.211	0.018	0.039	Calc.
Liquid ↔ BCC_A2 + Monocl.#1	Eutectic	325.4 ± 2.2	0.97 ± 0.01	1.00 ± 0.01	0.04 ± 0.01	Exp.
		325.7	0.974	1.000	0.037	Calc.
BCC_A2 ↔ AMPD-II + Monocl.#1	Eutectoid	353.6	0.002	0.000	0.003	Calc.
BCC_A2 + Monocl.#1 ↔ Monocl.#2	Peritectoid	233.6	1.000	0.005	0.995	Calc.

these sets of the parameters are shown in Fig. 1(a) and (b), respectively, including also the experimental data. Obviously, the resulted descriptions fit the experimental data properly.

It was found that the eutectic point is at 90.45 mol% SCN and 318.0 K in the NPG–SCN system and at 97.39 mol% SCN and 325.7 K in the AMPD–SCN system. In the NPG–SCN system the OCs/ODICs transformation occurs at a temperature of about 3 K lower than the temperature of the eutectic reaction (see Fig. 1(a)). That yields this binary system promising for applications as a model system for in situ observation of coupled eutectic growth with non-facetted phases. In the AMPD–SCN system the OCs/ODICs transition takes place at a temperature of about 29 K higher than the temperature of the eutectic reaction (see Fig. 1(b)). Therefore the eutectic reaction involves the liquid, the non-faceted BCC_A2 phase (ODICs) of SCN and the faceted monoclinic (OCs) phase of AMPD.

Fig. 2 shows the calculated phase diagrams of both systems including phase equilibria at sub-ambient temperatures. The sub-ambient equilibria result from thermodynamic modelling and were not proven experimentally within the frame of this work.

The calculated equilibria with the AMPD-II phase [2] in the AMPD–SCN system are presented in Fig. 3 and show very small temperature (~0.8 K) and composition (~0.4 mol% SCN) ranges for the stability of this phase.

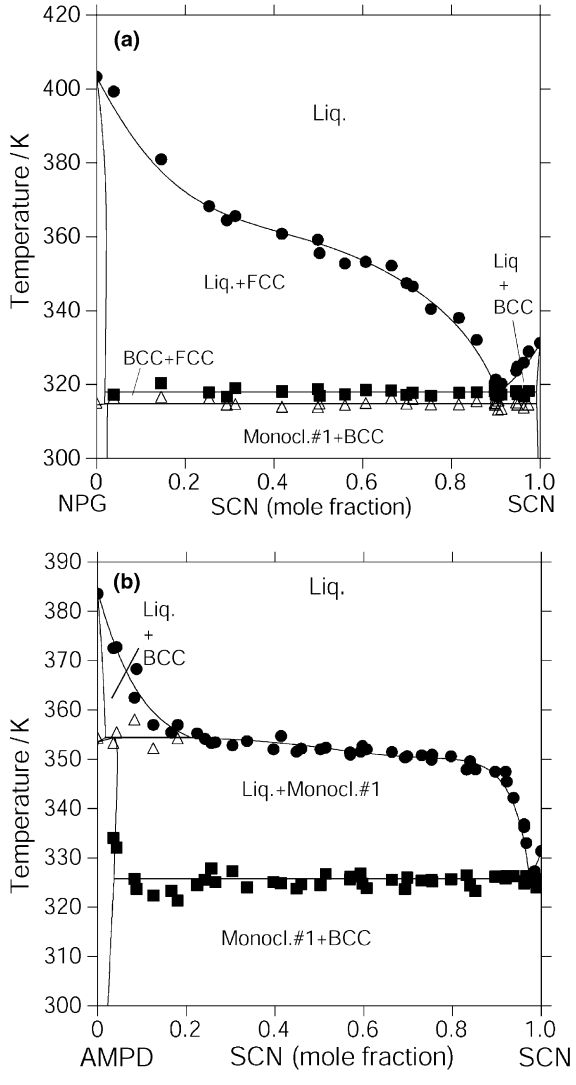

Fig. 1. Phase diagram of the binary system NPG–SCN (a) and AMPD–SCN (b) in the investigated temperature ranges: lines result from the present CALPHAD description; points are own experimental data.

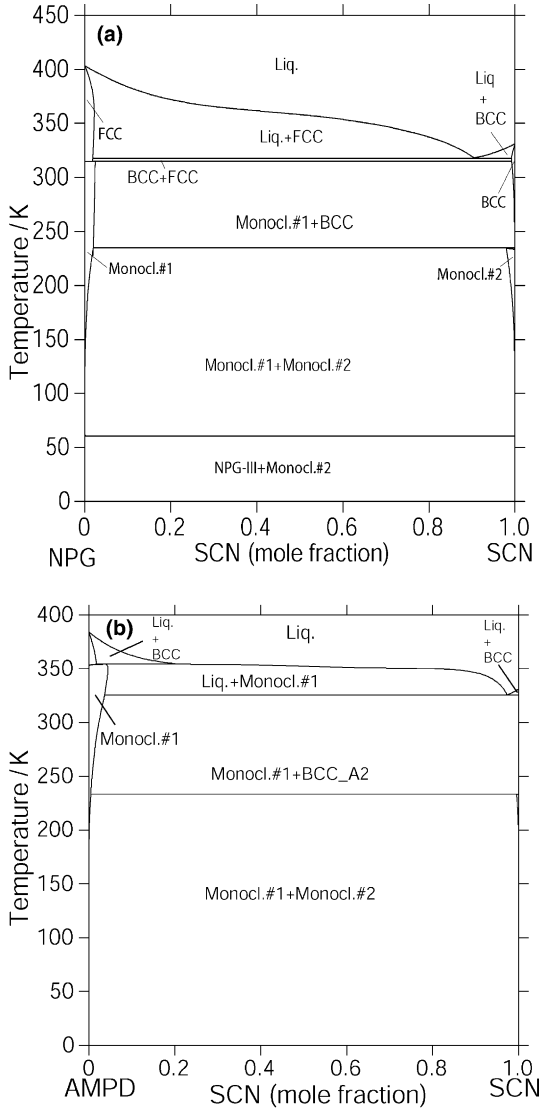

Fig. 2. Calculated phase diagram for the binary system NPG–SCN (a) and AMPD–SCN (b) including equilibria at sub-ambient temperatures.

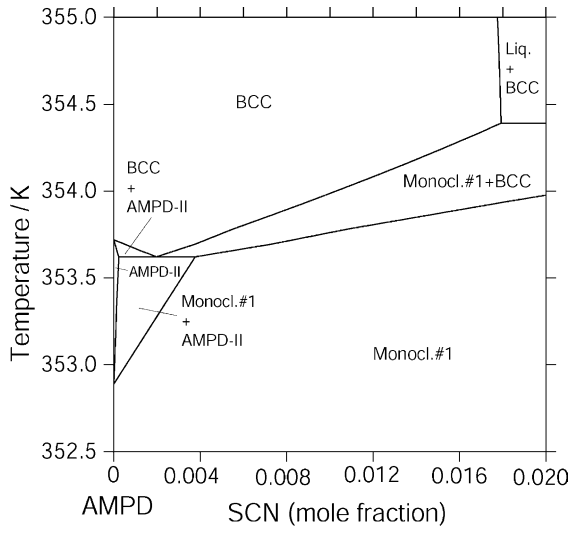

Fig. 3. Detail of calculated AMPD–SCN phase diagram showing non-variant transformation of the AMPD-II phase.

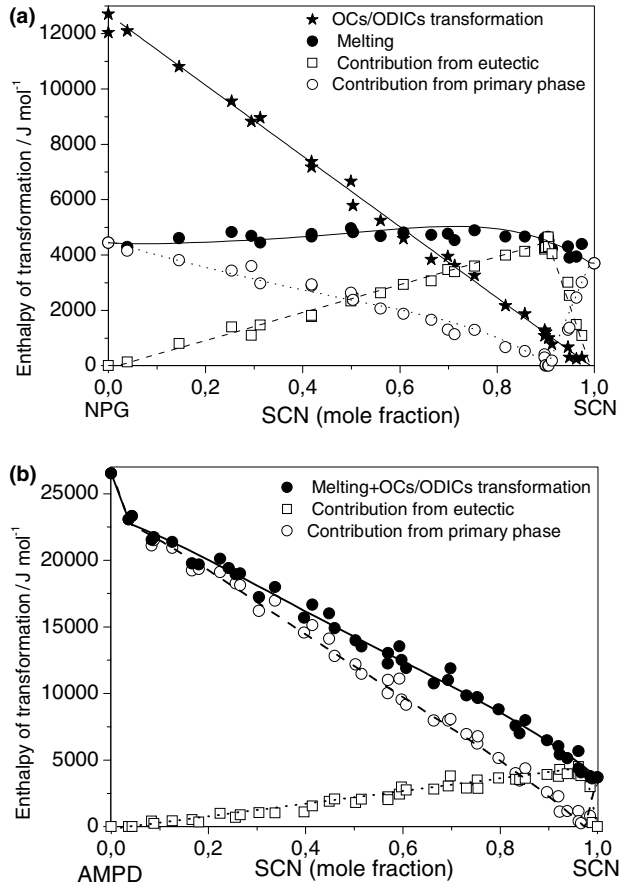

Fig. 4. Enthalpy of the OCs/ODICs transformation and enthalpy of melting for the NPG–SCN (a) and AMPD–SCN (b) system. Open points show the contributions of the primary phases and the eutectic. The points stem from own DSC measurements and the lines results from the present CALPHAD descriptions.

The calculated enthalpies of melting and the contributions of the primary phases and the eutectic to the enthalpies of melting for NPG–SCN and AMPD–SCN alloys are shown in Fig. 4(a) and (b), respectively. The calculated values match the experimental data obtained by the DSC measurements quite well. It is worth noting that the experimental enthalpy data were also very useful in earlier stages of optimisation: They were used for the evaluation of mutual solubility limits by straight line extrapolation of the enthalpy of OCs/ODICs transformation and also of the eutectic contributions to the enthalpy of melting. For example, in Fig. 4(a) the intersection points of these lines and the composition axes correspond to the solubility of SCN in NPG and of NPG in SCN at the temperatures of the relevant non-variant reactions. Sharp change of the slope of the composition dependency of the melting enthalpy in the AMPD–SCN system at ~4 at.% SCN (see Fig. 4(b)) also directly indicates the solubility limit of SCN in the BCC_A2 phase of AMPD at the eutectic temperature.

Fig. 5(a) and (b) shows the composition dependency of the enthalpy of formation of phases, as calculated from the present thermodynamic descriptions. For all phases

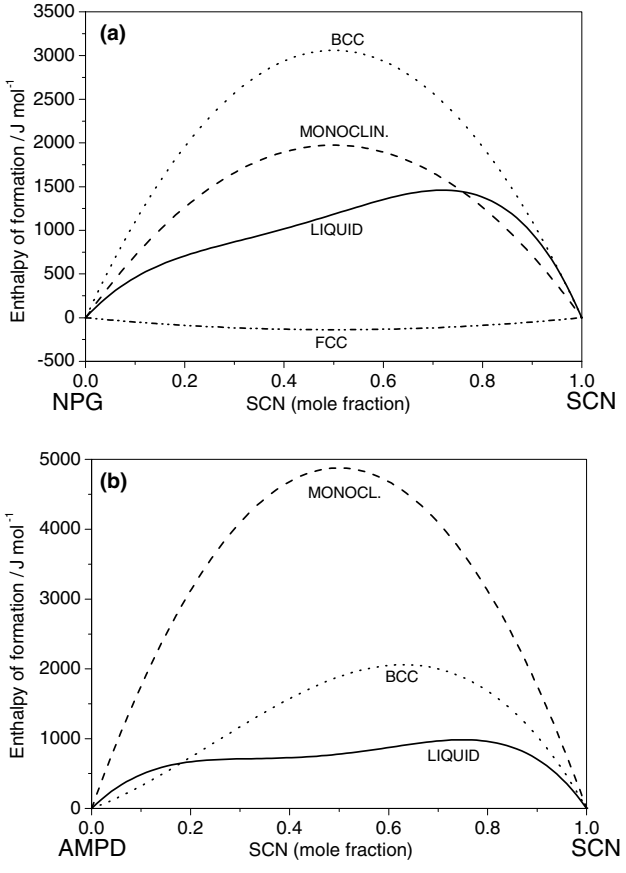

Fig. 5. Calculated integral enthalpy of formation of phases in the NPG–SCN (a) and the AMPD–SCN (b) system.

of both systems, except FCC_A1 in NPG–SCN, repulsive intermolecular interactions are dominant. From a thermodynamic point of view the FCC_A1 phase in NPG–SCN behaves practically close to ideal. The values were obtained by simultaneous optimisation of the enthalpies of melting of the alloys, solubility, the liquidus and the solidus data. This procedure leads to good values of the enthalpies of formation of phases relative to one another. However, their absolute values need to be checked by direct experimental methods, e.g., by calorimetry.

2.3. Unidirectional solidification

Unidirectional solidification experiments were performed after a previous equilibration of NPG–SCN and AMPD–SCN samples inside the Bridgman furnace, when a well defined interface between solid and liquid was established. For the experiments with NPG–SCN alloys flat glass cells with gap thickness of about 5–10 μm prepared according to [1] were used. For experiments with AMPD–SCN alloys rectangular glass capillaries with 300 μm in thickness, 4 mm in width and 120 mm in length were used. To provide homogeneous samples in such thin cells or capillaries, the liquid alloys were filled by vacuum sucking and kept in liquid state before applying the temperature gradient. Otherwise, when the equilibration in the Bridgman furnace was performed on solid samples a lot of small and randomly distributed bubbles formed inside the cells, probably due to large volume changes associated to the OCs/ODICs transformations.

2.3.1. NPG–SCN alloys

Fig. 6(a)–(c) shows the photographs of the stabilized interface after an equilibration time of 1 h for the hyper-eutectic alloy NPG–91.3 mol% SCN, for the eutectic alloy NPG–90.45 mol% SCN and for the hypo-eutectic alloy NPG–89.7 mol% SCN, respectively. In the hyper-eutectic alloy (Fig. 6(a)) a layer of about 50 μm length consisting of the primary phase of SCN (the BCC_A2 phase) can be observed. In the hypo-eutectic alloy (Fig. 6(c)) a layer of about 110 μm containing disk-like primary particles of the FCC_A1 phase of NPG is established, with the particles being non-facetted as well. In the eutectic alloy (Fig. 6(b)) the solidification of the liquid sample started with a regular rod-like eutectic structure. In the process of equilibration prior to solidification within the time of about 1h the phases coarsen at the solid/liquid interface while sharp and well-developed triple points form between the FCC_A1 (NPG), the BCC_A2 (SCN) and the liquid phases.

In the early stage of unidirectional solidification of the eutectic alloy a regular rod-like pattern starts to develop (Fig. 7(b)) and after 40 min of solidification under

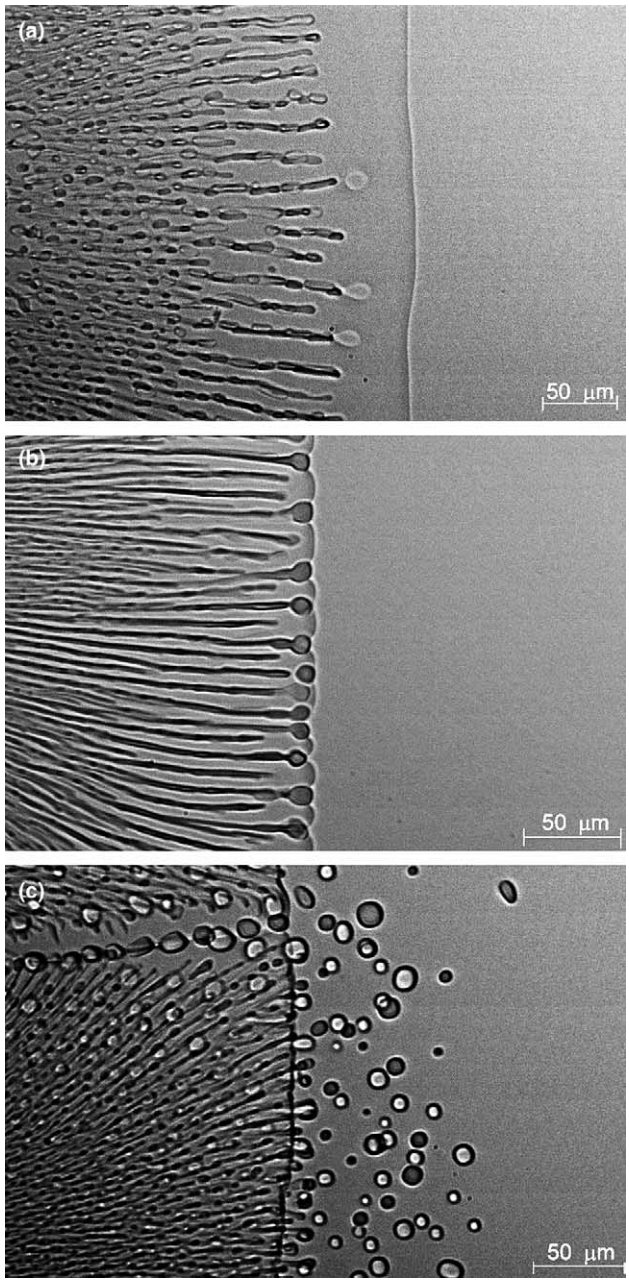

Fig. 6. Microstructure of selected NPG–SCN alloys prior to unidirectional solidification. The solid/liquid interface was stabilized from fully liquid samples and equilibrated inside the Bridgman furnace after 1 h under a temperature gradient $G = 4.5$ K mm^{-1} for the hyper-eutectic alloy NPG–91.3 mol% SCN (a), for the eutectic alloy NPG–90.45 mol% SCN (b) and for the hypo-eutectic alloy NPG–89.7 mol% SCN (c). Different brightness of the NPG particles is due to their different high level or focus positions.

the temperature gradient $G = 4.5$ K mm^{-1} and the pulling velocity $v = 0.10$ μm s^{-1} regular rod-like eutectic growth establishes. For the hyper-eutectic alloy a banded structure was observed for the same solidification conditions as above, where eutectic bands are separated by single phase bands of BCC_A2 (SCN). The banded structure shows a periodicity of about 150 μm

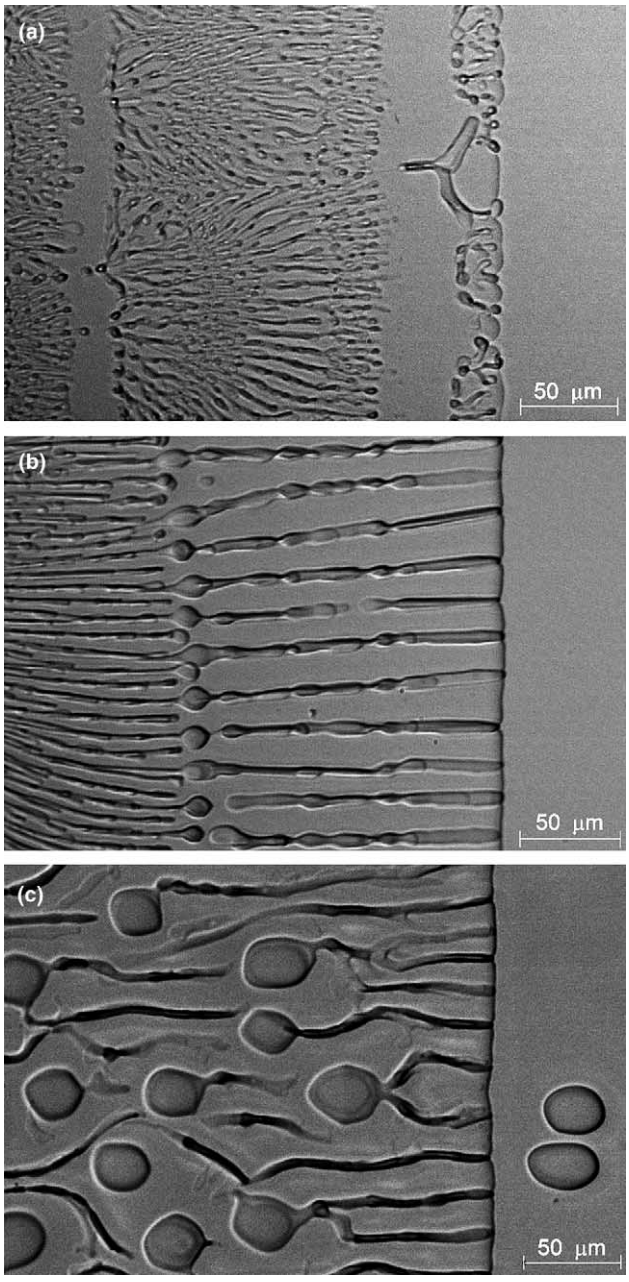

Fig. 7. The microstructures of the hyper-eutectic alloy NPG–91.3 mol% SCN (a), of the eutectic alloy NPG–90.45 mol% SCN (b) and of the hypo-eutectic alloy NPG–89.7 mol% SCN (c) during early growth show coupled growth establishing. The temperature gradient and the pulling velocity are $G = 4.5$ K mm^{-1} and $v = 0.10$ μm s^{-1}, respectively.

(Fig. 7(a)). Here it was observed that growth of eutectic bands starts from the BCC_A2/liquid interface after considerable undercooling via nucleation of the FCC_A1 phase of NPG.

For the case of the hypo-eutectic alloy (Fig. 7(c)) the primary disk-shaped NPG particles coarsen during early growth, interrupt rod growth and generate new grains consisting of several NPG rods. After overgrowing the region with primary NPG particles, steady-state solidification in this sample is achieved with regular coupled growth (Fig. 8). Here the microstructure is recorded in a region far from the solid/liquid interface close to the cooler of the Bridgman furnace: The black rods (see middle part of the Fig. 8) are due to the solid state transformation of NPG, namely the transition from the FCC_A1 (ODICs) to the monoclinic (OCs) phase.

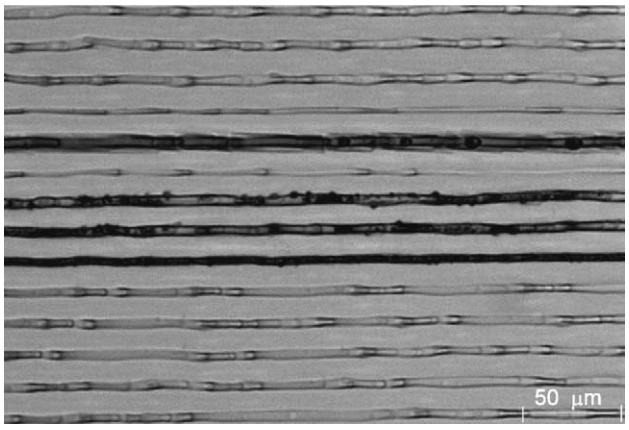

Fig. 8. Microstructure of the hypo-eutectic alloy NPG–89.7 mol% SCN after 12 h of unidirectional solidification with a pulling velocity $v = 0.10$ μm s^{-1} under the temperature gradient of 4.5 K mm^{-1} close to the cooler of the Bridgman furnace. Black regions in the middle part of the picture correspond to the FCC (ODICs)/monoclinic (OCs) transformation of the NPG rods.

It can be concluded, that in the NPG–SCN system coupled growth of two non-facetted plastic crystals occurs from the liquid of eutectic composition with a regular rod-like structure. The plastic crystals or ODICs are SCN with BCC_A2 structure and NPG with FCC_A1 structure. The eutectic pattern consists of 88 vol% SCN (BCC_A2 phase, matrix) and 12 vol% NPG (FCC_A1 phase, rods).

2.3.2. AMPD–SCN alloys

In Fig. 9(a)–(d) the photographs of the stabilized interface inside the Bridgman furnace are shown, corresponding to an equilibration time of 1 h for the eutectic alloy AMPD-97.4 mol% SCN with $G = 4.5$ K mm^{-1}, for the hypo-eutectic alloy AMPD-76.3 mol% SCN with $G = 5.9$ K mm^{-1}, for the hypo-eutectic alloy AMPD–57.2 mol% SCN with $G = 6.0$ K mm^{-1} and for the AMPD-rich alloy with 11.5 mol% SCN ($G = 7.5$ K mm^{-1}), respectively. In the eutectic alloy (Fig. 9(a)) the faceted monoclinic (AMPD) crystals protrude from the BCC_A2 (SCN) into the liquid. In the hypo-eutectic alloy AMPD-76.3 mol% SCN (Fig. 9(b)) a layer of the monoclinic long crystals protrude far into the liquid. In the hypo-eutectic alloy with 57.2 mol% SCN (Fig. 9(c)) a compact layer of facetted monoclinic crystals of the AMPD phase are

in equilibrium with the liquid phase. These observations agree well with the modelled phase diagram AMPD–SCN. The alloy AMPD–11.5 mol% SCN (Fig. 9(d)) shows a layer of about 400 μm consisting of BCC_A2 primary crystals (ODICs) ahead of the monoclinic crystals (OCs) that is also in good agreement with the obtained phase diagram (see Fig. 1(b)).

Unidirectional solidification of all the above AMPD–SCN alloys over distances of about 2 mm resulted in facetted crystal growth of the monoclinic AMPD-phase: The eutectic alloy solidified at $v = 0.1$ μm s^{-1} showed that the crystals formed during equilibration continued to grow without obvious change of shape or thickness (Fig. 10). The hypo-eutectic alloy AMPD-76.3 mol% SCN solidified at $v = 0.1$ μm s^{-1} formed well facetted and somewhat tilted crystals of AMPD (Fig. 11(a)). Increasing the pulling rate to $v = 1.0$ μm s^{-1} resulted in faster growth of monoclinic

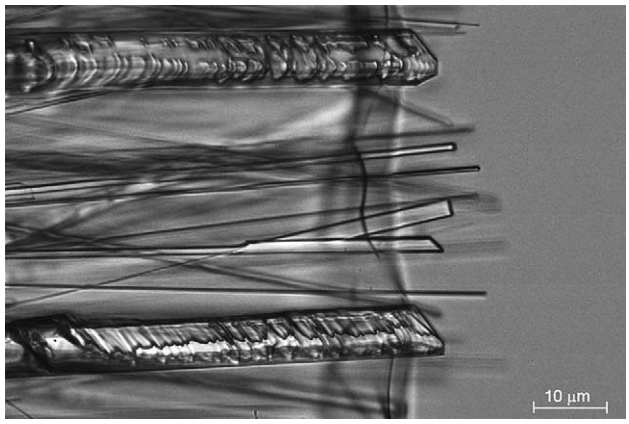

Fig. 10. The microstructure of the eutectic alloy AMPD–97.4 mol% SCN during early growth shows the faceted monoclinic crystals (AMPD) and non-facetted BCC_A2 phase (SCN) at the solid–liquid interface. The temperature gradient and the pulling velocity are $G = 4.5$ K mm^{-1} and $v = 0.10$ μm s^{-1}, respectively.

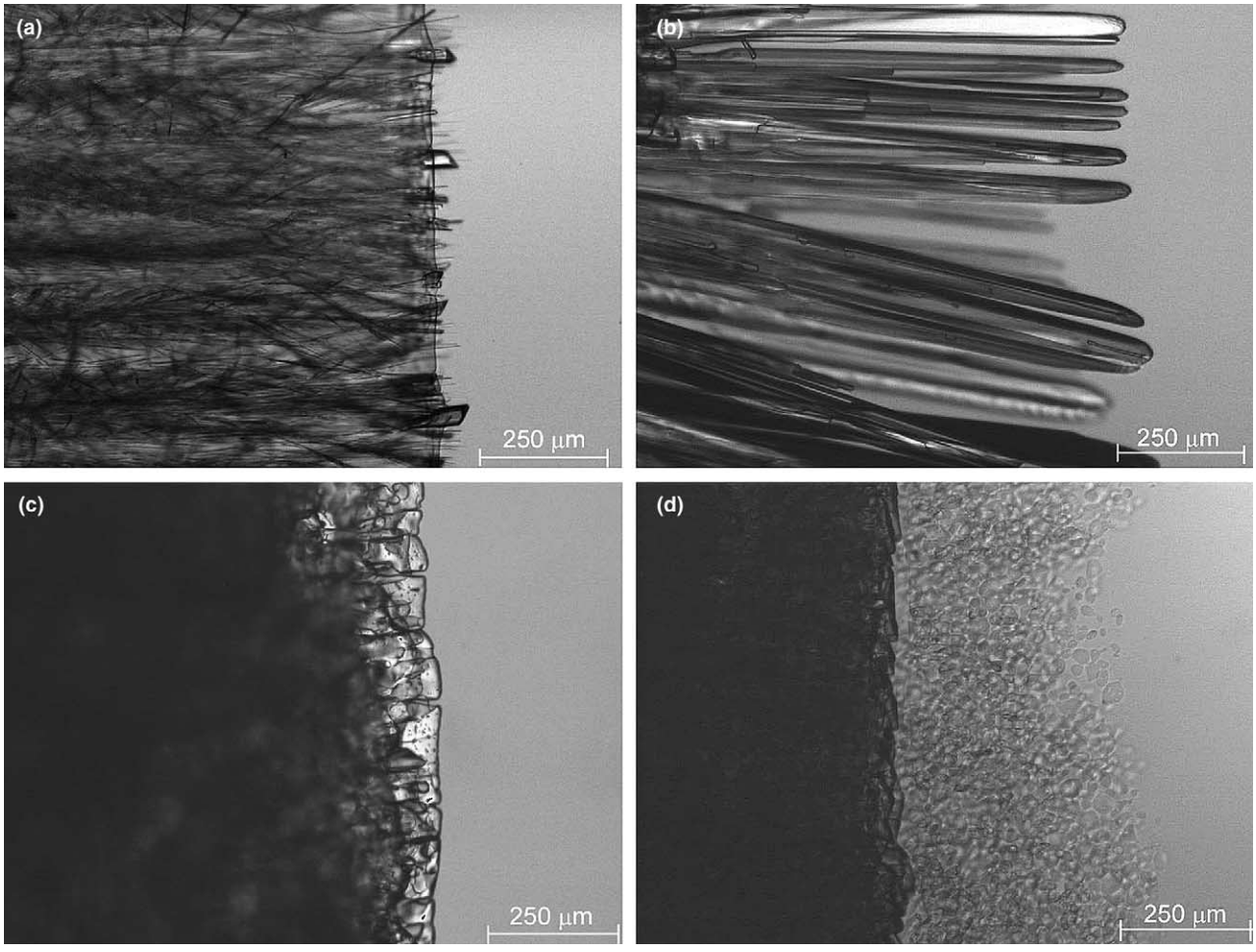

Fig. 9. Microstructure of the AMPD–SCN alloys prior to unidirectional solidification: The solid/liquid interface was equilibrated inside the Bridgman furnace for 1 h for the eutectic alloy AMPD–97.4 mol% SCN with $G = 4.5$ K mm^{-1} (a), for the hypo-eutectic alloy AMPD–76.3 mol% SCN with $G = 5.9$ K mm^{-1} (b), for the hypo-eutectic AMPD–57.2 mol% SCN alloy with $G = 6.0$ K mm^{-1} (c) and for the AMPD-rich alloy with 11.5 mol% SCN ($G = 7.5$ K mm^{-1}) (d).

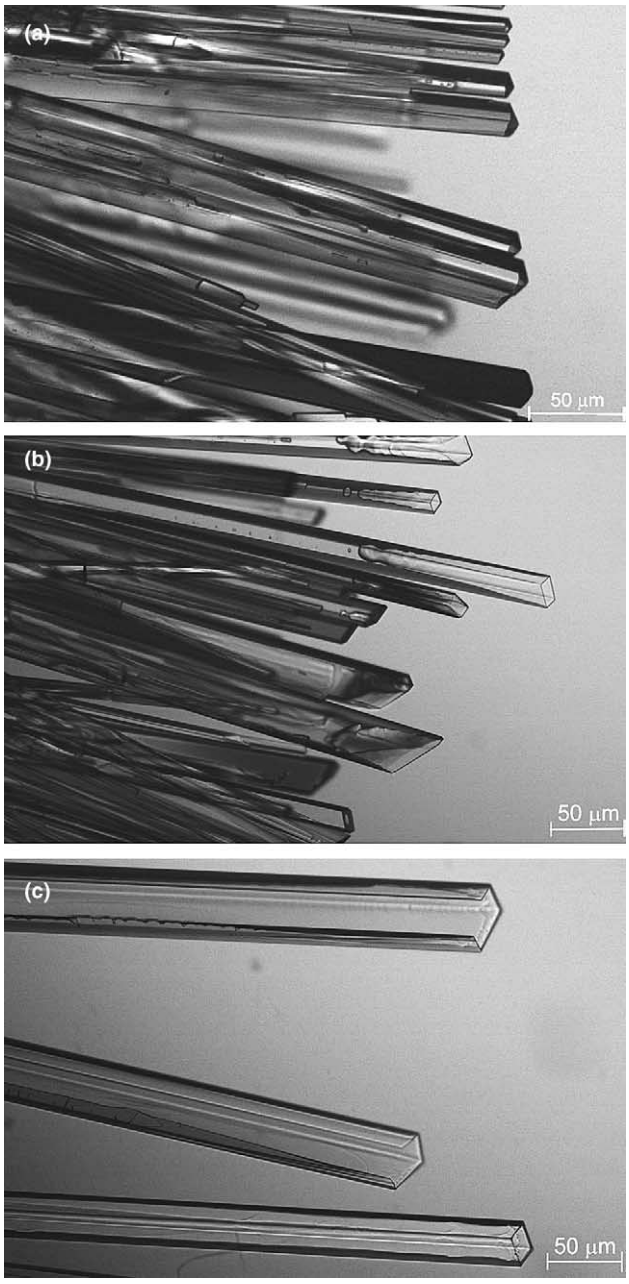

Fig. 11. Growth of the monoclinic crystals (AMPD) in hypo-eutectic alloy AMPD–76.3 mol% SCN under the temperature gradient of 5.9 K mm^{-1}: (a) pulling velocity is $v = 0.1$ μm s^{-1}; (b) pulling velocity changed from $v = 0.1$ to $v = 1.0$ μm s^{-1} and hollow crystals start to grow (see upper part of the picture); (c) continuing growth of the rectangular shaped capillaries and open profiles at pulling velocity $v = 1.0$ μm s^{-1}.

AMPD-crystals with rectangular shape in cross-section, which gradually transformed into rectangular shaped capillaries (hollow crystals) (see upper part of Fig. 11(b)). With time growth of these capillaries or open thin wall profiles was dominant (Fig. 11(c)). The hypo-eutectic alloy AMPD–57.2 mol% SCN solidified at $v = 0.1$ μm s^{-1} exhibited single phase growth of massive facetted monoclinic AMPD-crystals (Fig. 12).

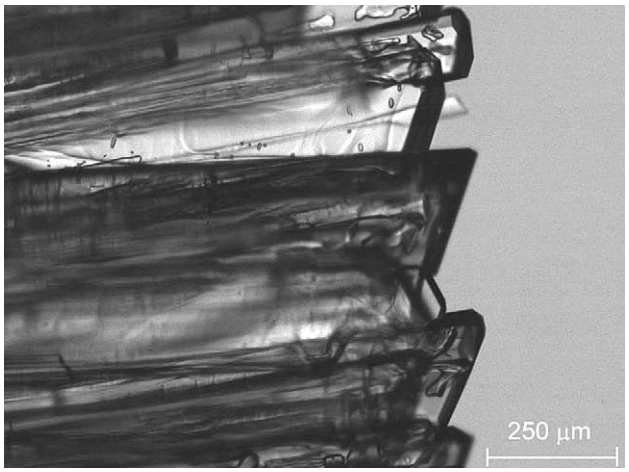

Fig. 12. Growth of the monoclinic crystals (AMPD) in hypo-eutectic alloy AMPD–57.2 mol% SCN under the temperature gradient $G = 6.0$ K $mm^{-1}$and the puling rate $v = 0.1$ μm s^{-1}.

3. Conclusions

The present work was dedicated to the thermodynamic description of the binary organic alloy systems neopentylglycol–succinonitrile (NPG–SCN) and amino-methyl-propanediol–succinonitrile (AMPD–SCN) by means of experimental and computational thermodynamics. The phase diagrams for the systems were modelled using the CALPHAD approach that simultaneously optimises experimentally determined thermodynamic data and data on phase equilibria. A proper agreement between experimental and calculated data for the phase diagrams as well as for the thermochemical properties was achieved. Experiments and calculations show that both systems NPG–SCN and AMPD–SCN exhibit a eutectic reaction with the eutectic point at 90.45 mol% SCN (318.0 K) and at 97.39 mol% SCN (325.7 K), respectively. In the NPG–SCN system this reaction occurs at a temperature of about 3 K higher than the temperature of the OCs/ODICs transition, and is thus promising for application as model systems for in situ observation of non-facetted coupled eutectic growth. Unidirectional solidification of the eutectic NPG–SCN alloys confirmed that coupled growth of two non-facetted phases occurs with a regular rod-like structure. Unidirectional solidification of the SCN-rich alloys of the AMPD–SCN system resulted in growth of the well faceted monoclinic crystals of AMPD, which transform with increasing puling rate into rectangular shaped capillaries or open thin wall profiles.

Acknowledgements

We gratefully acknowledge the funding of this work by the Deutsches Zentrum für Luft- und Raumfahrt DLR under Grant No. FKZ 50 WM 0043 and the

support by the European Space Agency ESA within the frame of the SETA-project. Thanks are due to the group of Dr. Faivre, Groupe de Physique des Solides (GPS), Université Paris6/7, France, for many fruitful discussions.

References

[1] Witusiewicz VT, Sturz L, Hecht U, Rex S. Acta Mater 2004;52:4561.
[2] Witusiewicz VT, Sturz L, Hecht U, Rex S. Acta Mater 2004;52:5071.
[3] Witusiewicz VT, Sturz L, Hecht U, Rex S. Acta Mater [accepted].
[4] Sturz L, Witusiewicz VT, Hecht U, Rex S. J Cryst Growth 2004;270:273.
[5] Wulff CA, Westrum Jr EF. J Phys Chem 1963;67:2376.
[6] Mangum BW, El-Sabban S. SMR 1970 NBS Special Publication 260-101.
[7] Zhang ZY, Zhou H, Yang ML. Gaodeng Xuexiao Huaxue Xuebao 1988;9:1085.
[8] Kamae R, Suenaga K, Matsuo T, Suga H. J Chem Thermodyn 2001;33:471.
[9] Zhang ZY, Yang ML. Thermochim Acta 1990;169:263.
[10] Dinsdale AT. CALPHAD 1991;15:177.
[11] Sundman B, Jansson B, Anderson J-O. CALPHAD 1985;9:153.